PERGAMON

International Journal of Multiphase Flow 27 (2001) 1127–1150

International Journal of Multiphase Flow

www.elsevier.com/locate/ijmulflow

Heat transfer and thermal pattern around a sphere in a turbulent boundary layer

G. Hetsroni *, C.-F. Li, A. Mosyak, I. Tiselj

Faculty of Mechanical Engineering, Technion – Israel Institute of Technology, Haifa 32000, Israel

Received 25 February 2000; received in revised form 11 November 2000

Abstract

Direct numerical simulation (DNS) is performed by solving the governing equations for fluid flow and heat transfer. The nondimensional sphere diameters are 17 and 34 wall units and cover several collocation points of the fluid. Two-way coupling is used to account for the effect of the sphere on the structure of the near-wall turbulence and the main stream. The calculation of the thermal field is done with the same grid system used for the velocity field. Water was used as test fluid, with the Prandtl number $Pr = 5.4$. The calculation is performed for a single stationary sphere attached to the bottom of the flume. The heat transfer calculations were carried out at a constant heat flux wall boundary condition. The present DNS results indicate essential enhancement of heat transfer coefficient associated with a flow motion toward the wall. The thermal pattern around the sphere is obtained and compared with the experimental images. A possible mechanism of heat transfer in the presence of coarse particles in the near-wall region of a turbulent boundary layer is discussed.

Keywords: Direct numerical simulation (DNS); Large solid particles; Near-wall turbulence; Heat transfer; Thermal pattern

1. Introduction

The scalar transport on a small moving particle or a particle attached to a flat surface and embedded in a shear flow, is not only interesting from a pure heat-mass transfer point of view, but also has many applications. Prediction of flow and heat transfer around bodies mounted on a surface is very important in relation to many types of heat exchangers and fluid machineries, and numerical investigations (Goldstein and Karni, 1984; Fisher and Eibeck, 1990; Chyu and

* Corresponding author. Tel.: +1-972-4-832-2058; fax: +1-972-4-832-4533.
E-mail address: hetsroni@tx.technion.ac.il (G. Hetsroni).

0301-9322/01/$ - see front matter
PII: S0301-9322(00)00068-9

Natarajan, 1991). The heat and mass transfer on particles in the neighborhood of surface is also important in the chemical industry where one is interested in the behavior of catalyst particle near a wall. Numerous experimental and numerical investigations have been reported on local heat-mass transfer distributions around an obstacle at Prandtl number $Pr = 1$. (Igarashi and Yamasaki, 1989; Davalath and Bayazitoglu, 1987; Morris and Garimella, 1996; Sparrow et al., 1984; Faghri and Asako, 1994; Nakajima and Ota, 1998). It is clear that heat transfer features strongly depend on the boundary layer characteristics.

Studies of heat (or mass) transfer for a flow around submerged objects are limited, particularly for cylinders, cubes and parallelepipeds (PPD) resting on a surface. Goldstein et al. (1985) used naphthalene sublimation to measure the local enhancement of transport in the vicinity of cylinders with varying height-to-diameter ratios. Ichimiya et al. (1988) examined heat transfer for flow around a cylinder for a range of cylinder dimensions and flow rates. Their general conclusions were in agreement with Goldstein et al. (1985). They also observed the presence of several local maxima in transport rates that were located immediately upstream and downstream from the cylinder. For flow around a submerged PPD, the experimental results of Dasgupta et al. (1993) observed local enhancement of the mass transfer. Schlosser et al. (1998) applied the methodology of Dasgupta et al. (1993) to measure mass transfer to the floor of a recirculating tank in the vicinity of a submerged parallelepiped. They presented a detailed map of mass transfer resistance over entire regions of a flat surface. Convective heat transfer induced by square and circular columns in turbulent channel flow was studied using liquid crystal thermography and computational fluid dynamics by Zhang et al. (1995). The numerical analysis was carried out by solving the governing equations for fluid flow and heat transfer using a finite-volume method. The Nusselt number distribution on the flat plate showed the heat transfer enhancement in the vicinity of the column. On the other hand, there has been no specific effort to predict heat or mass transfer patterns that result from flow around submerged spherical particle, perhaps because flow and temperature fields induced by such geometry reflect their complexity.

The present study is motivated by experimental studies carried out by Hetsroni and Rozenblit (1994) and Hetsroni et al. (1995). They used infrared (IR) thermography to study the thermal interaction between the particle-laden turbulent flow and a heated plate, and heat transfer enhancement by a sphere attached to the bottom of the flume. The measurement of the temperature field with the particle and without it showed that the heat transfer coefficient increased locally by a factor of 1.5–3, for a particle of the order of 10–25 wall units. A general decrease in the wall temperature was observed in the vicinity of the particle. Numerical simulation of the velocity field was performed by Li et al. (1999), and showed a significant influence of the particles on the mean flow and velocity fluctuations.

Detailed data on the effect of coarse particles, located on the wall, on heat transfer in a turbulent boundary layer, have been obtained by Hetsroni et al. (1997b). It was hypothesized that the increase in the heat transfer rate was due to the relative velocity between the particle and fluid near the wall, which caused an in rush of cold fluid into the wall region. Recently Hetsroni et al. (2001) studied the effect of particle motion on turbulence and heat transfer and compared the results to those produced by a stationary particle. It was shown that enhancement of the heat transfer coefficient depends on the ratio of the particle Reynolds number (based on the particle diameter and relative velocity), to the shear Reynolds number, based on the particle diameter and shear velocity. Results of these experiments showed that the effect of particle motion and rotation on the

increase of heat transfer coefficient in the turbulent boundary layer at high particle Reynolds number, $Re_P > 100$, is the same as for a stationary particle. In these experiments the velocity field was not studied. The present study aims to fill this gap. For this purpose the present DNS were carried out at two high particle Reynolds numbers based on particle diameter and mean flow velocity at the center of the particles, $Re_P = 120$ and $Re_P = 370$. As a result we obtain detailed information on the velocity field and temperature field on the wall for the case when the effect of the particle on heat transfer is maximized. To our knowledge, it is the first time that thermal pattern on the heated wall is calculated by DNS. The purpose of the present study is to examine this effect and to predict details of heat transfer around a sphere submerged in a flume by direct numerical simulation (DNS). We aim to calculate the temperature distribution in a turbulent boundary layer of water flow at $Pr = 5.4$. At this Prandtl number the temperature boundary layer is embedded in the so-called viscous sublayer. This is the region of turbulent boundary layer nearest to the wall. As the name suggests, the flow in this layer is dominated by viscous forces. However, the flow is also influenced by the turbulence above the viscous sublayer and therefore is highly non-stationary. This means that apart from a mean temperature distribution around the particle, we can also expect strong temperature fluctuations both in time and space. The latter is especially important when one needs information on the coherent thermal structures. Therefore, information on thermal pattern at the heated wall is also the goal that we pursue in this study.

2. Mathematical description

2.1. Flow field

We examine in some detail the two-way coupling and interaction between large particles ($Re_p > 1$) and the turbulence in the near-wall region of the open channel turbulent flow. We use Lam and Banerjee (1988) method of DNS of flow field.

The time-dependent, three-dimensional Navier–Stokes and continuity equations are solved in a rectangular domain. The flow geometry and coordinate system are sketched in Fig. 1. The streamwise direction is denoted by x_1, the spanwise direction by x_2, and the wall-normal direction

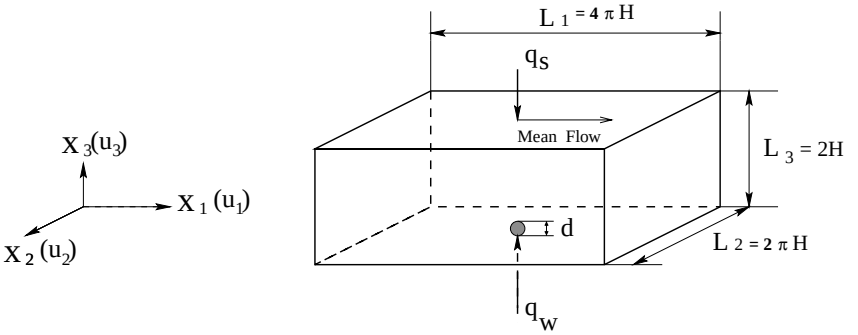

Fig. 1. Configuration of present DNS: computational domain and coordinate system.

by x_3, while the velocity components are u_1, u_2, u_3, correspondingly. The flow is driven by a constant streamwise pressure gradient. The governing equations for the flow field are

$$\frac{\partial u_i^+}{\partial x_i^+} = 0, \tag{1}$$

$$\frac{\partial u_i^+}{\partial t^+} + u_j^+ \frac{\partial u_i^+}{\partial x_j^+} = -\frac{\partial p^+}{\partial x_i^+} + \frac{\partial^2 u_i^+}{\partial x_j^+ \partial x_j^+}. \tag{2}$$

The equations have been made dimensionless by using wall variables, the friction velocity u_τ and the kinematic viscosity ν. The friction velocity u_τ, which in terms of the wall shear stress, τ_w, and the fluid density, ρ, is defined as $u_\tau = (\tau_w/\rho)^{1/2}$, where $u_i^+ = u_i/u_\tau; x_i^+ = x_i u_\tau/\nu$; p is the pressure, $p^+ = p/\rho u_\tau^2$; t is the time, $t^+ = t u_\tau^2/\nu$. The Reynolds number Re_τ is defined as $Re_\tau = u_\tau\ 2H/\nu$ based on the friction velocity u_τ, and the full channel depth $2H$.

The boundary conditions are $u_1^+ = u_2^+ = u_3^+ = 0$ (no-slip) at the bottom wall, and $\partial u_1^+/\partial x_3^+ = \partial u_2^+/\partial x_3^+ = 0, u_3^+ = 0$ at the free surface. Periodic boundary conditions are imposed in streamwise (x_1) and spanwise (x_2)-directions. The initial conditions are the mean profiles for the velocity superimposed with sinusoidal perturbations.

A pseudo-spectral method (Hussaini and Zhang, 1987) is employed to solve the governing equations. In the homogeneous (x_1- and x_2)-directions, all the quantities are expressed by Fourier expansions. In the wall-normal direction x_3, which is nonhomogeneous, they are represented by Chebyshev polynomials.

In the present study, the turbulent channel flow of Reynolds number $Re_\tau = 171$ is simulated. The bulk Reynolds number $Re_B = 2Hu_B/\nu$ in this case is about 2600, where $2H$ is the flow depth, $2H = 37$ mm, and u_B is the bulk streamwise velocity. The calculations were carried out in a computational domain of $L_1^+ \times L_2^+ \times L_3^+ = 1074 \times 537 \times 171$ wall units in the x_1-, x_2- and x_3-directions with a resolution of $128 \times 128 \times 65$. A nonuniform distribution of collocation points is used in the wall-normal (x_3)-direction due to the nature of the Chebyshev polynomials, and the first collocation point away from the wall is at $x_3^+ = 0.1$.

After the flow field is brought to a stationary state, the sphere of diameter $d^+ = 17$ or $d^+ = 34$ is introduced into the flow, where $d^+ = du_\tau/\nu$, d is the sphere diameter. In the present study we simulate the cases of flow and heat transfer around a single sphere attached to the bottom. When the sphere is small, in the sense that $Re_p \ll 1$, the effect of the sphere on the flow field can be fed back explicitly at every time-step through a point force acting on the fluid. Such small sphere is of subgrid size, and therefore the force has to be distributed to the surrounding mesh points, see Pan and Banerjee (1996). In the present simulation $Re_p \gg 1$ and the sphere should cover enough collocation points in the fluid to get a detailed resolution of the flow pattern around a coarse particle. The sphere of $d^+ = 17$ occupied two nodes in the x_1-direction, and four nodes in the x_2-direction. The number of nodes occupied by a particle in the x_3-direction (normal to the bottom of the channel), takes up to 14 nodes near the wall when the sphere is touched to the bottom. For the sphere $d^+ = 34$, the occupied nodes are 4, 8 and 19 in the x_1-, x_2- and x_3-direction, respectively.

Two-way coupling is introduced as follows: all the velocities in the collocation points occupied by the sphere were made to be zero by using Eq. (2) with an additional source term S_{pi}. This source term is introduced into Eq. (2),

$$\frac{\partial u_i^+}{\partial t^+} + u_j^+ \frac{\partial u_i^+}{\partial x_j^+} = -\frac{\partial p^+}{\partial x_i^+} + \frac{\partial^2 u_i^+}{\partial x_j^+ \partial x_j^+} + S_{pi}. \tag{3}$$

A successful method for modeling of the no-slip boundaries with an external force field for the pseudo-spectral numerical scheme was described by Goldstein et al. (1993), who suggested the following external force in the collocation points p on the particle boundary:

$$\rho S_{pi}(x_p, t) = -\alpha \int_0^t u_i(x_p, t')\,\mathrm{d}t' - \beta u_i(x_p, t). \tag{4}$$

This force acts like a spring force on the fluid of mass $\rho\,\mathrm{d}x^3$ in point x_p, with spring constant α and the damping β. The time integral in Eq. (4) was approximated as a Riemann sum

$$\int_0^t u_i(x_p, t')\,\mathrm{d}t' \approx \sum_{j=1}^{N} u_i(x_p, j) \tag{5}$$

and the stability limit for Adams–Bashfort time marching, which imposes a constraint for the constants α and β, was given by

$$\Delta t < \frac{\sqrt{\beta^2 + 2\alpha k} - \beta}{\alpha}, \tag{6}$$

where k was a problem-dependent constant of order 1.

The problem of the upper approach is the detailed specification of the constants α, β, and k, and time keeping of the integrals Eq. (5). We have profited from the fact, which is not straight forward, that the upper approach works also for $\alpha = 0$. The recommended value of the constant β is in that case $\beta = 1/\Delta t$ and there is no need for the evaluation and keeping of the integrals Eq. (5).

One discrete time step of Eq. (3) was split into two substeps (LeVeque, 1992). In the first substep all velocities in the collocation points inside the particle are set to zero. This is equivalent to solving of the equation

$$\frac{\mathrm{d}u_i^+}{\mathrm{d}t} = -\beta u_i \tag{7}$$

with $\beta = 1/\Delta t$ and first-order time discretization. Results of this sub-step present input for the second sub-step in which the Navier–Stokes and continuity equations without source term are solved with standard pseudo-spectral method.

2.2. Temperature field

The thermal problem to be considered is the same as that in the experiments of Hetsroni and Rozenblit (1994) and Hetsroni et al. (1995, 1997b). The bottom wall is heated at a constant flux, and the free surface is considered as an adiabatic surface. The dimensional energy equation is

$$\frac{\partial T}{\partial t} + u_j \frac{\partial T}{\partial x_j} = \alpha \frac{\partial^2 T}{\partial x_j \partial x_j}, \tag{8}$$

where T is the temperature, α is the thermal diffusivity. The boundary conditions are heat flux $q_w = constant$ on the bottom wall, and heat flux $q_s = 0$ at the free surface. In spanwise (x_2)-direction, the periodic condition is imposed. We also carried out calculations with a constant temperature wall boundary condition to compare present method with previous DNS updated in the literature.

One should be taking into account the difference between isothermal and isoflux wall boundary conditions. The heating condition of the constant mean heat flux along the bottom of the flume, is equivalent to an assumption that the wall temperature ensemble-averaged over the x_2-direction and time should increase linearly in the x_1-direction (Kasagi et al., 1992). As a result, the bulk mean temperature should also increase linearly in the x_1-direction. The mean temperature gradient in x_1-direction can be expressed with wall heat flux, if the global energy balance is written for the averaged conditions in the channel volume $2HL_1L_2$, heated bottom surface L_1L_2 and in time which the fluid travelling with the bulk velocity u_B crosses the distance L_1

$$(2HL_1L_2)\rho c_p \Delta T = q_w 9L_1L_2)(L_1/u_B). \tag{9}$$

So the mean temperature gradient is

$$\Delta T/L_1 = q_w/(2H\,\rho c_p u_B). \tag{10}$$

The bulk velocity is defined as

$$u_B = \frac{1}{2H}\int_0^{2H} \langle u_1 \rangle_{x_1,x_2,t}\,\mathrm{d}x_3, \tag{11}$$

where $\langle u_1 \rangle_{x_1,x_2,t}$ means averaging over x_1, x_2, and time t. Usually the temperature transforms to $\theta = \langle T_{w,x_1} \rangle - T(x_1, x_2, x_3, t)$, and dimensionless temperature is defined as

$$\theta^+ = [\langle T_{w,x_1} \rangle - T9x_1, x_2, x_3, t)]/\theta_\tau, \tag{12}$$

where $\langle T_{w,x_1} \rangle$ is ensemble temperature along x_2-direction on the bottom wall and time at x_1 position. θ_τ is the friction temperature $(\theta_\tau = q_w/c_p u_\tau)$. For periodic boundary condition in the streamwise (x_1)-direction, the governing equation for the thermal field is given as follows (Kasagi et al., 1992; Kawamura et al., 1998)

$$\frac{\partial \theta^+}{\partial t^+} + u_j^+ \frac{\partial \theta^+}{\partial x_j^+} - \frac{u_1^+}{2u_B^+} = \frac{1}{Pr}\frac{\partial^2 \theta^+}{\partial x_j^+ \partial x_j^+}, \tag{13}$$

where $u_B^+ = u_B/u_\tau$, $Pr = \nu/\alpha$ is the Prandtl number. The last term on the left-hand side of Eq. (13) corresponds to the mean temperature gradient in x_1-direction. In the wall-normal (x_3)-direction, the dimensionless boundary condition is $\partial\theta^+/\partial x_3^+ = Pr$ at the bottom wall, and $\partial\theta^+/\partial x_3^+ = 0$ at the free surface.

When a flow is unsteady, there occur unsteady temperature fluctuations on the wall surface. The thermal streaky structures have been observed to exist on the walls in the experimental investigations (Iritani et al., 1984; Hetsroni and Rozenblit, 1994; Hetsroni et al., 1995), in which an open channel water flow was heated from the bottom with a constant heat flux. The temperature fluctuations may be determined by the coupled unsteady heat conduction inside the wall, so that they cannot be specified without knowing the wall material and its thickness. This conjugate heat transfer problem was studied by Kasagi et al. (1989). The particular case of wall thickness $\delta = 0$ corresponds to ideally isoflux wall with infinitesimally small wall thickness. One of the ingredients

in understanding turbulent transport of a scalar, between a flowing fluid and a solid surface, is the behavior of the fluctuating temperature on the heated wall. The usual approach is to consider the system as fully developed velocity and temperature fields when the heated wall is held at constant temperature. A DNS for the isoflux wall boundary condition was carried out by Kasagi et al. (1992), where the temperature fluctuations were assumed to be zero on the wall. The DNS assumption that the wall temperature fluctuations are zero, cannot explain the existence of the thermal pattern on the heated solid wall. In the present study DNS was performed under condition that wall temperature fluctuations are not zero, and the results are compared with the experimental data. The case of an ideal isoflux is used in the present study, to estimate those wall temperature fluctuations that could be realistically expected for a very thin wall.

Any buoyancy effect was neglected, and hence temperature was considered as a passive scalar. As the initial condition, a uniform temperature field was projected on the velocity field. The heat transfer simulation was started after the velocity field had reached a steady state. Then once the velocity field was calculated at each time step, the temperature field was obtained by integrating the energy equation with the same grid system used for the velocity field. For spatial discretization, the finite-control-volume method was used with second-order accuracy. The convection and diffusion terms were dealt by central differencing scheme. The Crank–Nicolson method was used for time advancement in connection with the time-step for DNS velocity field. By the finite volume method one can avoid the periodic boundary conditions in the streamwise direction. So the finite volume method allows one to obtain the development of thermal boundary layer in the streamwise direction. The finite difference method was used in DNS of thermal boundary layers recently performed by Kong et al. (2000). The particle causes significant changes in the velocity and the scalar fields. We studied this phenomenon, assuming that the thermal conductivity of the particle plays no role in the mechanism of heat transfer, i.e., we consider the particle as a turbulent promoter. We assure there is no heat transfer between the sphere and the fluid. The thermal boundary condition on the sphere surface is heat flux $q = 0$. We assume that all material and fluid properties are constant, so that the hydrodynamic results obtained earlier may be employed directly in the heat transfer analysis.

It should be noted that the velocity field is solved by pseudo-spectral method. However, spectral method has its disadvantages in comparison with finite-difference methods and finite volume methods, i.e., they are inflexible with respect to thermal boundary conditions. The DNS studies of heat transfer often did not employ a pseudo-spectral method, see Kawamura et al. (1998) and Lu and Hetsroni (1995). In these studies the system is considered as the fully developed velocity and temperature fields that exist in the boundary layer in which the heated wall is held at constant temperature. However, the most realistic situation of heat transfer from the solid wall corresponds to the isoflux wall boundary condition. This case is considered in the present study. On the other hand, we also carried out DNS with the isothermal wall boundary condition, to compare with the previous studies.

The computation proceeded until the temperature field was estimated to be fully developed. Next, the procedure was started in order to obtain statistical data about the temperature. Finally, the instantaneous temperature fields were used as an initial database for the main computation after all statistical quantities were obtained. The grid resolution, the time increment and all the schemes of the preliminary computation were the same as those in the main computation. The time integration was repeated for about 2500 ν/u_τ^2 and then the computation was further

continued for about 700 v/u_τ^2 (20,000 time steps) in order to calculate turbulence statistics as ensemble averages over space and time. The data sampling was started when we observed stationary time histories of the statistics.

3. Results and discussion

3.1. Validation of the temperature field simulation

To exploit DNS of turbulent heat transfer around a sphere placed in a turbulent boundary layer, the numerical accuracy of DNS should be first confirmed. In particular, the velocity field should have been well examined before any argument in the heat transfer aspect is put forward. The profiles of the mean velocity and root-mean-square (RMS) intensities were calculated by Li et al. (1999) and agreed well with previous DNS, reported by Kim et al. (1987). In the present study, the verification has been made for the turbulent heat transfer from the bottom of a flume.

3.1.1. Constant temperature wall boundary condition

In Fig. 2, the present DNS of turbulent heat transfer under a constant wall temperature condition have been compared to the data obtained by Kawamura et al. (1998) for $Pr = 5.0$. The mean temperature profile is shown in Fig. 2(a), where the dimensionless temperature Θ^+, normalized by the Prandtl number, Pr, is plotted vs the dimensionless wall-normal distance from the heated wall, x_3^+. The RMS of the temperature fluctuations, $\theta^+_{\mathrm{RMS}}/Pr$, vs x_3^+ is shown in Fig. 2(b). The values of streamwise turbulent heat flux, $u_1^+\theta^+/Pr$, and wall-normal turbulent heat flux, $u_3^+\theta^+/Pr$, are also examined and the results are shown in Figs. 2(c) and (d), respectively. In Figs. 2(a)–(d) the present DNS and the DNS of Kawamura et al. (1998) are shown by the solid lines and circles, respectively. In general, these statistical quantities are in very close agreement. Some discrepancies at x_3^+ about 100 could be due to the different thermal wall boundary conditions. It should be noted that Kawamura et al. (1998) performed simulation of turbulent heat transfer in a two-dimensional channel flow, where thermal boundary conditions are imposed at two walls.

3.1.2. Constant heat flux wall boundary condition

Fig. 3 shows the distribution of dimensionless mean temperature, Θ^+, in the wall-normal direction, x_3^+, under a constant heat flux wall boundary condition. The present results are compared with experimental data reported by Zukauskas and Slanciauskas (1987). The agreement is good for the conductive sublayer ($\Theta^+ = Prx_3^+$). For the logarithmic region, the present results are higher than that obtained experimentally by Zukauskas and Slanciauskas. It should be noted that the present simulation was performed at constant fluid physical properties. The experiments of Zukauskas and Slanciauskas were carried out at considerable difference between fluid physical properties in the viscous sublayer and in the logarithmic region. As was pointed out in their study, the temperature profiles in the logarithmic region should be shifted down compared to the case of constant fluid physical properties.

The RMS of the temperature fluctuations on the wall is quite different from zero under this constant heat flux wall boundary condition, as shown in Fig. 4. Intensity of temperature fluctuations in the wall-normal direction obtained in the present study was compared with the model

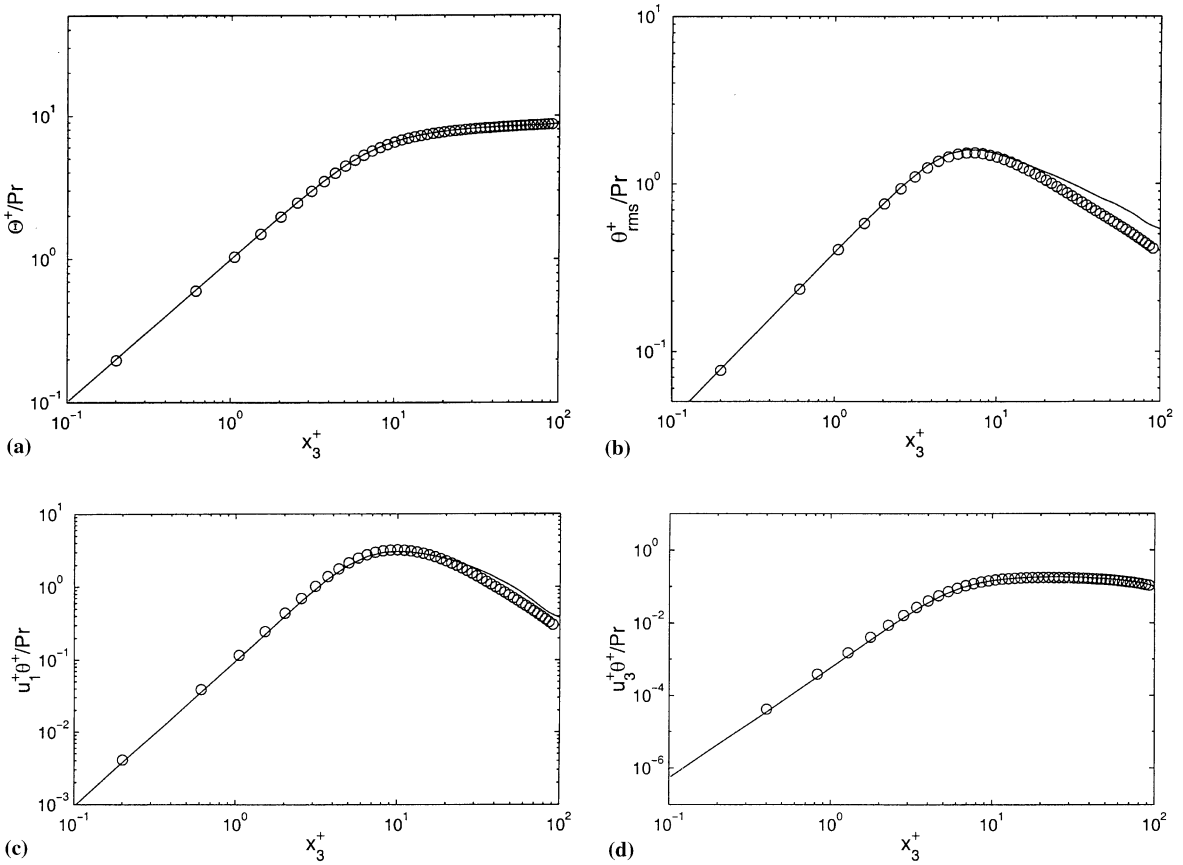

Fig. 2. Comparison of turbulent statistical quantities under a constant temperature wall boundary condition: (–) present DNS, $Pr = 5.4$, $Re_\tau = 171$; (○) Kawamura et al.'s DNS (1998), $Pr = 5.0$, $Re_\tau = 180$. (a) Nondimensional mean temperature profile. (b) Intensity of temperature fluctuations. (c) Streamwise turbulent heat flux. (d) Wall-normal turbulent heat flux.

results of Kasagi et al. (1989). In spite of different methodology (in present study we did not involve any turbulent model), the behavior in the near-wall region and the location of peak RMS temperature fluctuation are in agreement.

Fig. 5 shows the spanwise two-point correlations of temperature and streamwise velocity fluctuations in near-wall region. It can be seen that the first minimum associated with streaky structure is observed at the spanwise nondimensional distance (normalized by wall units) $\Delta x_2^+ = 50$ for both quantities. One can conclude that the average dimensionless streak spacing for near-wall flow coherent structures as well for wall temperature fluctuations is close to the value of $\lambda^+ = 100$, which are in good agreement with the well-known results (Iritani et al., 1984; Kim et al., 1987; Hetsroni and Rozenblit, 1994).

The agreement between Kawamura et al. (1998) and present DNS was achieved also for wall-normal and streamwise turbulent heat flux, cross-correlation function between streamwise velocity and temperature fluctuations, cross-correlation function between wall-normal velocity and

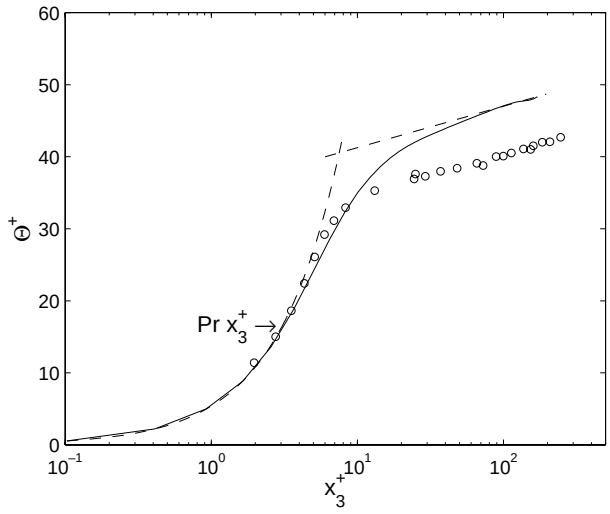

Fig. 3. Nondimensional mean temperature profile under a constant heat flux wall boundary condition: (–) present DNS; (○) Zukauskas and Slanciauskas (1987).

temperature fluctuations, as shown by Tiselj et al. (2000). Auto-correlation function of temperature fluctuations in the streamwise direction agree well with Kasagi et al. (1992).

For $Pr = 5.4$ the resolution of the present study in the streamwise and spanwise directions is approximately 1.8 times finer than that used by Na and Hanratty (2000) for $Pr = 10$. In the DNS study of heat transfer at $Pr = 10$, Na and Hanratty (2000) used 15 and 7.5 viscous length in the streamwise and spanwise directions, respectively. The validation of computational solution per-

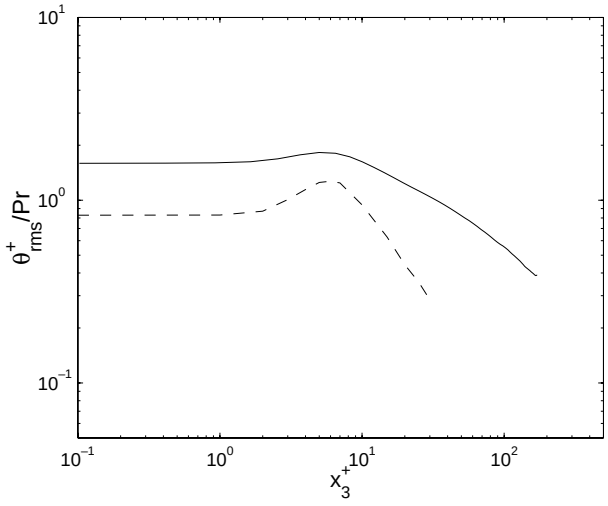

Fig. 4. Nondimensional intensity of temperature fluctuations under a constant heat flux wall boundary condition: (–) present DNS, $Pr = 5.4$; (- - -) model of Kasagi et al. (1989), $Pr = 7$.

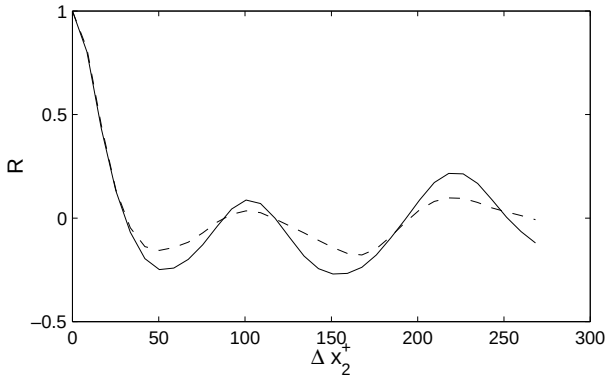

Fig. 5. Spanwise two-point correlations: (–) correlation of temperature fluctuation on the wall; (- - -) correlation of fluctuation of streamwise velocity near the wall (on the plane $x_3^+ = 5$).

formed in the present study showed that the resolution – 8.4 and 4.2 viscous length in the streamwise and spanwise directions, is fine enough to capture the significant small scale of the temperature field at $Pr = 5.4$. So that the resolution and accuracy of the present finite volume method is fine enough to obtain the first and second-order statistics.

3.2. Velocity and temperature field

3.2.1. Velocity distribution around the sphere

The plane view of partial computational mesh system is shown in Fig. 6(a). The circles represent the spheres of diameter $d^+ = 34$ and 17, respectively. The center of the spheres is located at the position $x_1^+ = 507.1, x_2^+ = 253.5$. Line 1 indicates streamwise axis of symmetry, and lines 2–6 indicate several spanwise cross-section lines at different distances from the center of the sphere. The spanwise view of partial grids near the bottom wall surrounding the sphere is shown in Fig. 6(b). Because the spheres are stationary on the bottom wall, the center of the spheres in normal coordinate are $x_3^+ = 17$ and $x_3^+ = 8.5$ for the sphere $d^+ = 34$ and 17, respectively.

Typical flow features associated with the flow around the sphere $d^+ = 34$ are shown in Fig. 7 for the views in the $x_1^+ - x_3^+$ and $x_1^+ - x_2^+$ plane (Fig. 7(a) and (b), respectively). The vector velocities show that the sphere affects the region about one diameter before the sphere, and a large area behind the sphere. For a free stream relative to a front of the sphere two areas may be defined: the flow along the sphere surface in the positive x_3^+-direction (measured from the front stagnation point) and the flow in the negative x_3^+-direction. The flow in the positive x_3^+-direction accelerates from the front stagnation point and reaches a maximum velocity at the top of the sphere. The flow in the negative direction decelerates from the stagnation point and reaches a zero velocity at the bottom. The sphere Reynolds number $Re_P = U_C d/v$ (based on the mean flow velocity at the center of the sphere) is 370, and recirculating flow behind the sphere is clearly seen. A small recirculating flow can also be found before the sphere. For the sphere of diameter $d^+ = 34$, it was found that a change in the streamwise component of the flow velocity in the front of the sphere, and strong disturbances behind the sphere, take place in the region from $x_1^+ = 450$ to $x_1^+ = 650$. The velocity fields around the sphere $d^+ = 34$ and the sphere $d^+ = 17\,(Re_P = 120)$ are

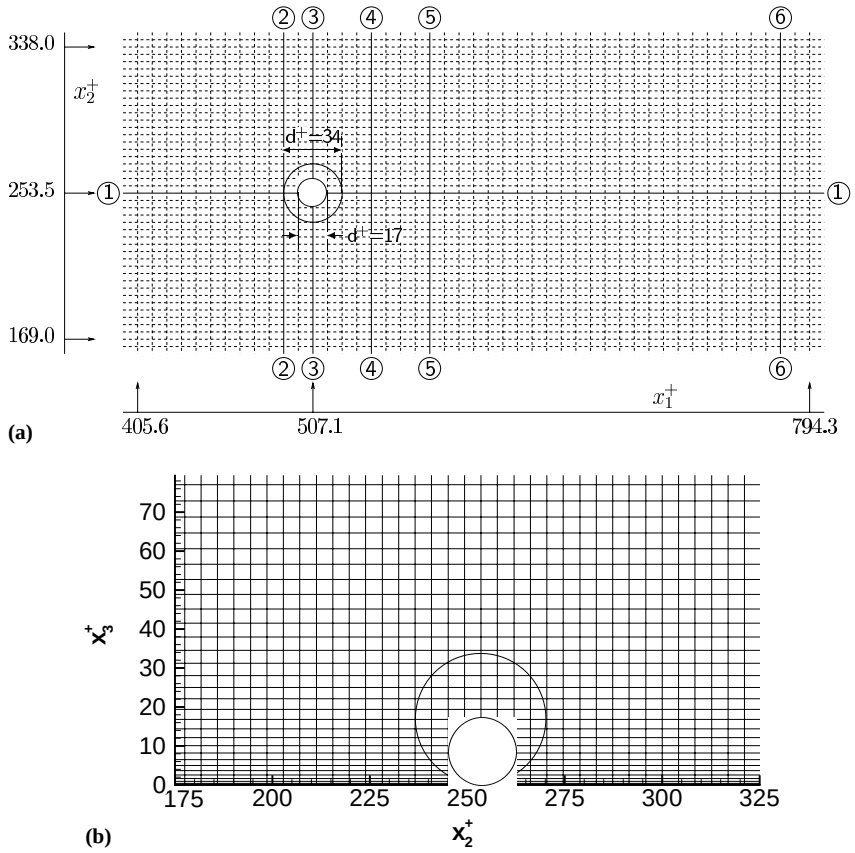

Fig. 6. Computational mesh system and the sphere location at the bottom of the flume: (a) view in the $x_1^+ - x_2^+$ plane; (b) view in the $x_2^+ - x_3^+$ plane.

presented in this region in Figs. 7 and 8. In these figures the ratio of x_{1C}/d is also shown for comparison. Here x_{1C} is the distance from the center of the sphere in the streamwise direction. The comparison of Figs. 8 and 7 clearly demonstrates that in the front of the sphere $d^+ = 17$ the disturbances are weaker than that for the sphere $d^+ = 34$. In the wake region behind the sphere $d^+ = 17$, the negative flow velocities were almost not observed.

3.2.2. Temperature distribution in the spanwise direction at the bottom of the flume

Let us consider this effect for the sphere $d^+ = 34$, since for the sphere $d^+ = 17$ it is qualitatively the same. Fig. 9 shows the temperature T distribution (assuming that the mean flow water temperature is 20°C) vs x_{2C}/d at different spanwise cross-sections indicated in Fig. 6(a) (x_{2C} is the spanwise distance from the sphere center position touched on the wall). Consider the wall temperature behavior along the axis of the sphere symmetry in the streamwise direction, the temperature decreases from the distance about one diameter before the center of the sphere, and reaches the minimum value at the distance $x_{1C}/d = -0.5$ (Fig. 9(a), x_{1C} is the streamwise distance from the sphere center position touched on the wall). This can be explained by a cooler flow

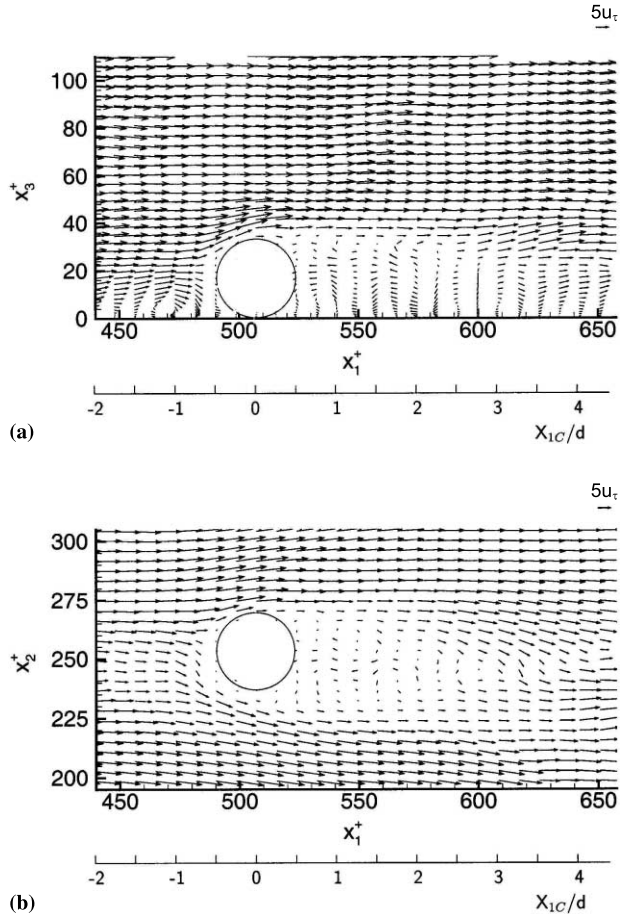

Fig. 7. Velocity distribution around the sphere $d^+ = 34$, $Re_P = 370$ $u_\tau = (\tau_w/\rho)^{1/2}$: (a) in the $x_1^+ - x_3^+$ plane ($x_2^+ = 253.5$); (b) in the $x_1^+ - x_2^+$ plane ($x_3^+ = 17.0$).

motion from the outer layer toward the wall. In the region $-0.5 < x_{1C}/d < 0$ the velocity decreases, and bottom temperature increases up to maximum value at $x_{1C}/d \sim 0$ (Fig. 9(b)). In the region $0 < x_{1C}/d < 2$ the strong temperature fluctuations are observed (Figs. 9(c) and (d)). Then the temperature fluctuations are weaker, and the averaged wall temperature increases (Fig. 9(e)).

3.3. Heat transfer coefficients

Heat transfer coefficients were calculated along the axis of symmetry of the sphere in the streamwise direction. The normalization was performed with the time and space averaged heat transfer coefficient, α_0 , which was derived from the average heat flux and bottom temperature without sphere. The governing equation for the thermal field (Eq. (13)) is derived using the friction reference temperature θ^+ (Eq. (12)). The heat transfer coefficient is defined as follows:

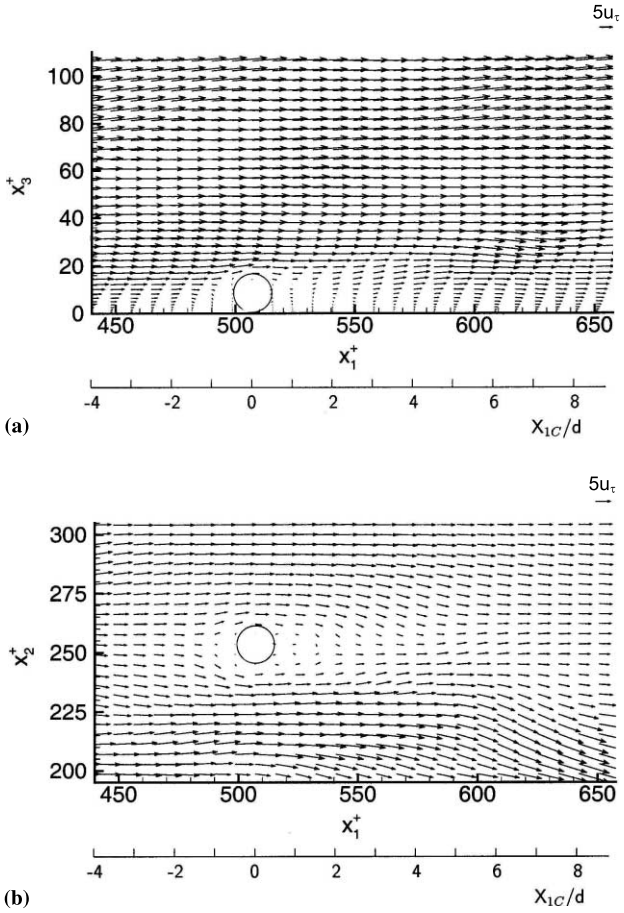

Fig. 8. Velocity distribution around the sphere $d^+ = 17$, $Re_P = 120$ $u_\tau = (\tau_w/\rho)^{1/2}$: (a) in the $x_1^+ - x_3^+$ plane ($x_2^+ = 253.5$); (b) in the $x_1^+ - x_2^+$ plane ($x_3^+ = 8.5$).

$$\alpha = \frac{\rho c_p u_\tau}{\langle \theta^+ \rangle}.$$

Here $\langle \theta^+ \rangle$ is the bulk reference temperature, i.e., averaged in the cross-section area of the flume in time and space. In Fig. 10, the time averaged DNS results of normalized heat transfer coefficient along the streamwise sphere symmetry line (line 1) for the sphere $d^+ = 17$ are compared with experimental results of Hetsroni et al. (1995). The present calculation agrees well with experiments. The front and side flow regions cause intense heat removal which results in a rise of the heat transfer. At $x_{1C}/d \sim -0.5$ the first maximum of heat transfer coefficient is observed. Then the heat transfer coefficient decreases up to the first minimum at $x_{1C}/d \sim 0$. In the region of $0 < x_{1C}/d < 2$ the flow in the near bottom region, despite recirculations, prevented intense heat removal which resulted in a local decrease of the heat transfer coefficient. These features are more pronounced if the sphere diameter increases.

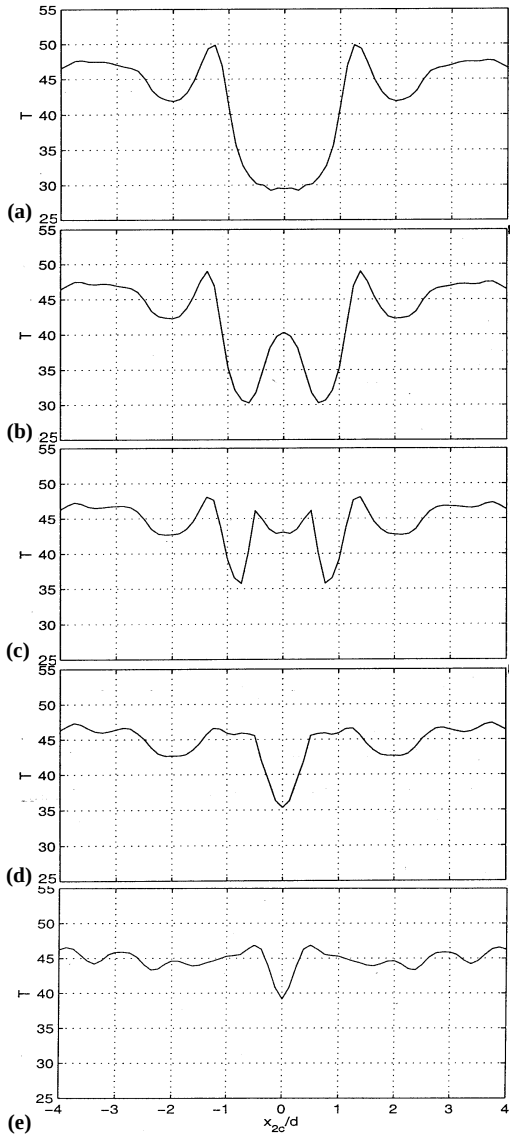

Fig. 9. Temperature distribution along different spanwise cross-section lines, $d^+ = 34$, $Re_P = 370$, $Pr = 5.4$: (a) along line 2, $x_{1C}/d = -0.5$; (b) along line 3, $x_{1C}/d = 0$; (c) along line 4, $x_{1C}/d = 1$; (d) along line 5, $x_{1C}/d = 2$; (e) along line 6, $x_{1C}/d = 8$.

In the present study the heat transfer in turbulent water flow in the flume (an open channel) was studied. To examine DNS results a comparison was performed with experimental data obtained in water flow in a flume. We compared the results of the present study ($Pr = 5.4$) to results ($Pr = 55$) reported by Li et al. (2000). Although the temperature distribution on the heated wall for both cases is qualitatively similar, the quantitative comparison showed marked differences. Because the temperature boundary layer is much thinner in the case of $Pr = 55$, compared to the case of

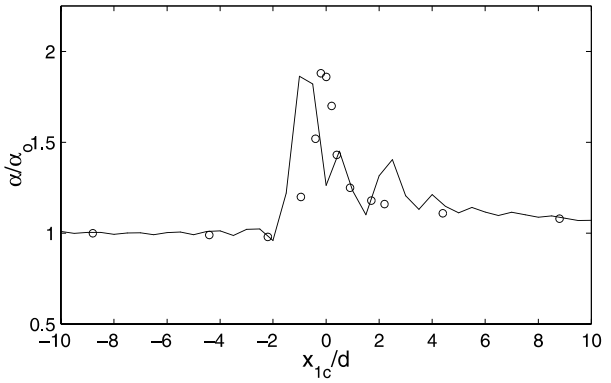

Fig. 10. Comparison between numerical and experimental results of normalized heat transfer coefficient along the streamwise sphere symmetry line (line 1), $d^+ = 17$: (–) present DNS, $Re_B = 2600$, $Pr = 5.4$; (○) Hetsroni et al. (1995), $Re_B = 8650$, $Pr = 7.1$.

$Pr = 5.4$, the corresponding peak of heat transfer coefficient is higher for $Pr = 55$. For both cases between the first and second peak, a minimum of heat transfer coefficient was observed. For $Pr = 55$, this minimum and the second peak are also more pronounced than that for $Pr = 5.4$.

Normalized time averaged heat transfer coefficients along the streamwise axis of the sphere symmetry for $d^+ = 34$ are shown in Fig. 11. It can be seen that the local peak of heat transfer enhancement is up to 2.8, much higher than that for small sphere $d^+ = 17$ (Fig. 10). The heat transfer coefficients fluctuate behind the sphere to a great extent due to the recirculating flow. The influenced wake area is also much longer for the sphere $d^+ = 34$.

3.4. Effect of the sphere on thermal pattern and temperature fluctuations at the heated wall

Figs. 12(a) and (b) depict the typical instantaneous thermal field of the heated wall, i.e., in the $x_1^+ - x_2^+$ plane at $x_3^+ = 0$, near the location of the sphere. The flow moves from left to right. The

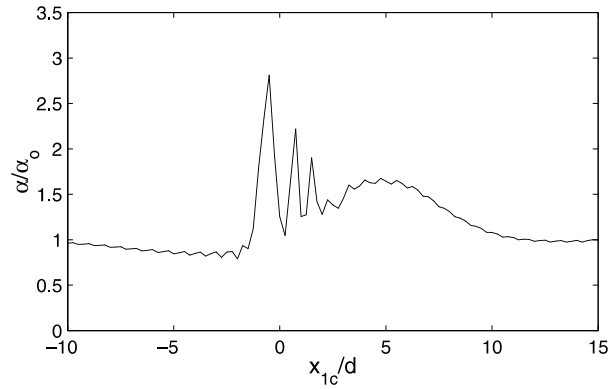

Fig. 11. Numerical results of normalized heat transfer coefficient along the streamwise sphere symmetry line (line 1), $d^+ = 34$, $Re_P = 370$, $Re_B = 2600$, $Pr = 5.4$.

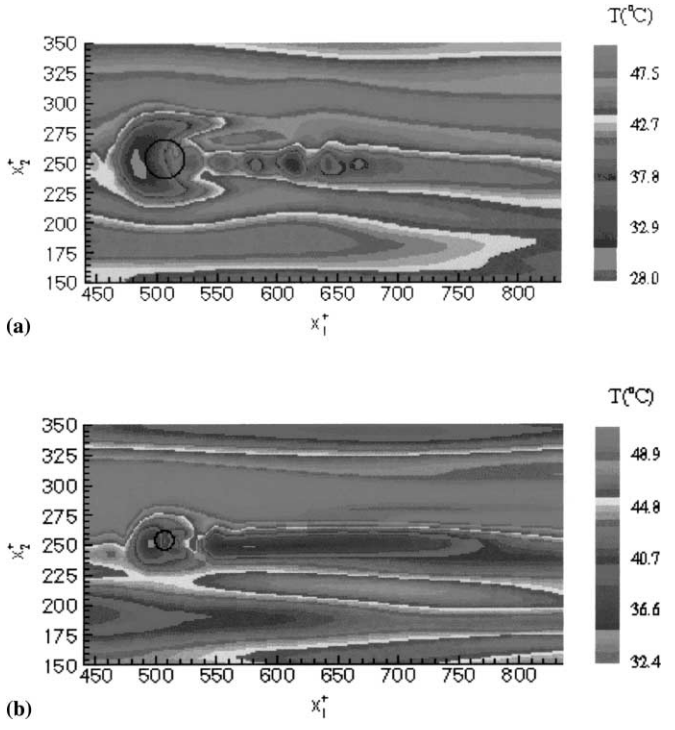

Fig. 12. Visualization of the instantaneous thermal pattern on the heated wall: (a) $d^+ = 34$, $Re_P = 370$, $Pr = 5.4$; (b) $d^+ = 17$, $Re_P = 120$, $Pr = 5.4$.

color shades are proportional to the temperature, and thus reveal the colder region in the front of the stationary sphere. In Fig. 12(a) ($d^+ = 34$) the number of thermal spikes on the heated wall is clearly observed in the wake region. For the sphere of $d^+ = 17$ (Fig. 12(b)) the spikes are almost not observed. This issue will be discussed later.

Figs. 13(a) and (b) indicate the RMS of temperature fluctuations on the heated wall along the streamline to the center of the sphere (line 1), for the spheres $d^+ = 34$ and $d^+ = 17$, respectively. In the wake region, the maximum value of the RMS of temperature fluctuations is higher for the sphere $d^+ = 34$ than that for the sphere $d^+ = 17$. These results are in agreement with the experimental observation by Hetsroni et al. (1995).

4. Discussion

4.1. Lift force

To estimate the lift force in a shear flow, Kurose and Komori (1999) derived the expression:

$$C_L = 5.816\left(\frac{|\gamma^*|}{Re_P}\right)^{1/2} - 0.875\gamma^*, \tag{14}$$

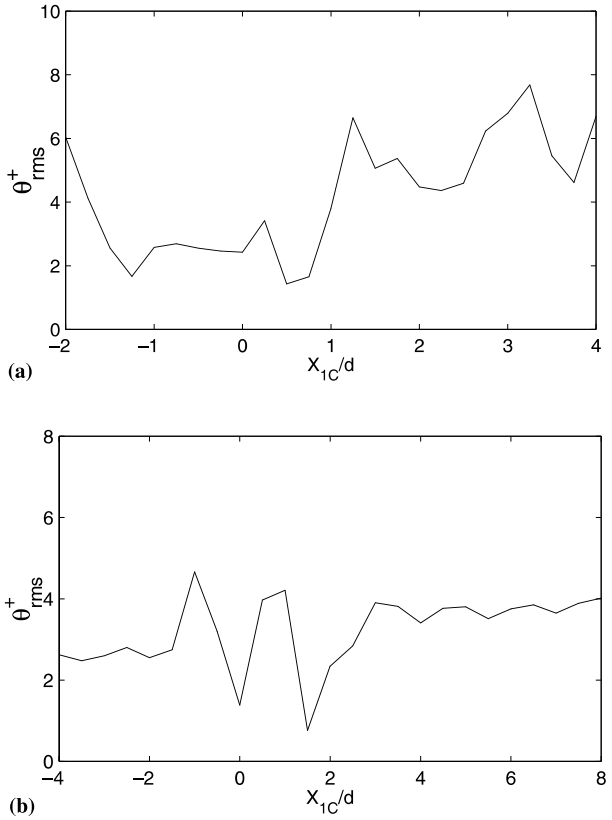

Fig. 13. RMS of wall temperature fluctuation in the streamwise direction (line 1): (a) $d^+ = 34$, $Re_P = 370$, $Pr = 5.4$; (b) $d^+ = 17$, $Re_P = 120$, $Pr = 5.4$.

where C_L is the lift coefficient, γ^* is the dimensionless shear rate of the fluid,

$$\gamma^* = \frac{d^+}{2U_C^+}\frac{\partial U^+}{\partial y^+},$$

and U_C^+ is the mean velocity of the fluid on the streamline through the center of the sphere normalized by shear velocity u_τ. In the present study γ^* is about 0.4 and 0.7 for the sphere $d^+ = 34, Re_P = 370$ and sphere $d^+ = 17, Re_P = 120$, respectively. Under these conditions the lift coefficient C_L has a negative value.

In previous studies, carried out for a small sphere in linear shear flows (Saffman, 1965; McLaughlin, 1991), the lift force has been considered to act from lower-fluid-velocity side to the higher-fluid-velocity side. The negative value of C_L means that the lift force acts from the higher-fluid-velocity side to the lower-fluid-velocity side. As is shown by Kurose and Komori (1999) the negative lift force is attributed to the flow separation behind the sphere, at high particle Reynolds numbers, $Re_P > 100$.

4.2. Effect of bulk Reynolds number and centrifugal force on the flow behind the sphere

To clarify effect of bulk Reynolds number on instantaneous temperature distribution on the heated wall in the region of the wake behind the sphere, we compare DNS results for $d^+ = 34$ at $Re_B = 2600$ (Fig. 14(a)) to experimental one for $d^+ = 33$ at $Re_B = 8650$ (Fig. 14(b)). The $x_1^+ - x_2^+$ plane of high and low temperature regions at $x_3^+ = 0$ obtained from the present DNS is shown in Fig. 14(a) under heat flux $q_w = 10^4$ W/m^2. Fig. 14(b) gives the thermal field of the heated foil near the spherical particle of diameter $d^+ = 33$ at $Re_B = 8650$, and heat flux $q_w = 10^4$ W/m^2, obtained in experimental study by Hetsroni et al. (1995). The flow moves from the bottom to the top.

Comparing Figs. 14(a) and (b) one should take into account that experiments were performed at the bulk Reynolds number $Re_B = 8650$, while the DNS was carried out at $Re_B = 2600$. In the experiments (Hetsroni et al., 1995), the sphere was made of stainless steel and its conductivity affected the thermal pattern in the vicinity of the sphere. In contrast to the DNS, in the experi-

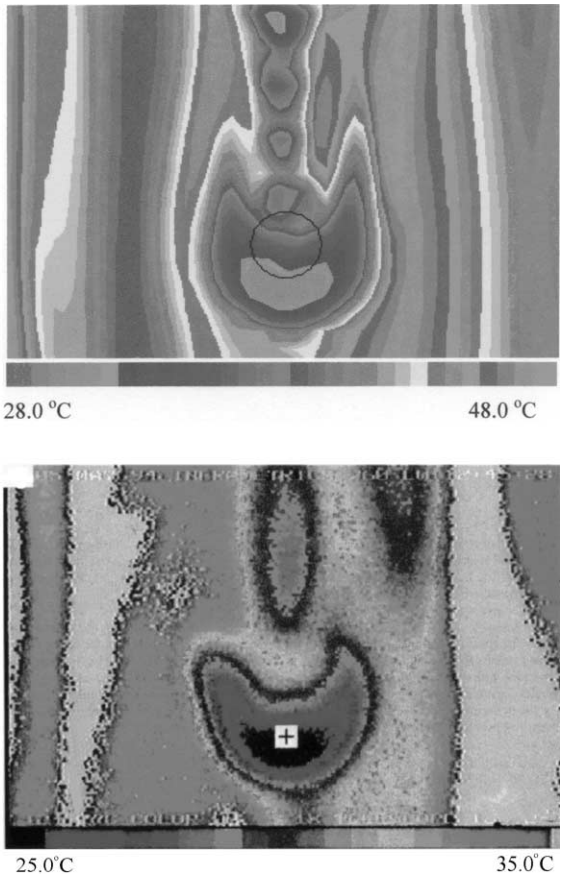

Fig. 14. Effect of the bulk Reynolds number on instantaneous thermal pattern on the heated wall. Comparison DNS to experimental results. The flow direction x_1 is from the bottom to the top and the dimensionless width of the figure is $\Delta x_2^+ = 250$: (a) DNS results, $d^+ = 34$, $Re_P = 370$, $Re_B = 2600$, $Pr = 5.4$; (b) experimental results, $d^+ = 33$ (located at '+' position), $Re_B = 8650$, $Pr = 7.1$.

mental study the fluid properties were not constant. In the experiments the constant heat flux wall boundary condition was achieved using stainless foil of thickness 0.05 mm. The foil was heated by DC current, and the IR image of the heater was recorded by an IR Radiometer. The DNS were carried out for ideally isoflux wall with infinitesimally small wall thickness.

We consider a possible mechanism of the effect of a single sphere on the rate of heat transfer in a turbulent boundary layer. Suppose that a sphere of diameter d is attached to the heated wall. It is well known that in a stationary curved flow the centrifugal forces acting on a fluid element are balanced by a centripetal pressure gradient, which causes modulation of turbulent fluctuations affecting the heat transfer. These effects manifest themselves also in the zone of interaction of the wake behind the coarse particle and the near-wall flow (Fig. 15). Depending on the distribution of the radial pressure gradient, it enhances or suppresses turbulent fluctuations and, accordingly, increases or decreases the heat transfer. Detailed analysis of this phenomenon was performed by Hetsroni et al. (1997b). In the case when centrifugal forces enhance, the radial component of the fluctuations and the heat transfer coefficient increase. In the case when centrifugal forces suppress, the radial component of the fluctuations and the heat transfer coefficient decrease. This effect determines the spikes in heat transfer coefficient in the domain behind the particle, and the temperature distribution on the heated wall. From a physical point of view, such a sphere may affect the rate of heat transfer at a point B (see Fig. 15) in two ways: by changing the value of the velocity, or as a result of a change in the direction of the velocity vector. This effect is determined by the ratio of the diameter of the sphere d to the height of the fluid layer $2H$. For small value of $d/2H$, the effect of centrifugal forces is small. Comparing Fig. 12(a), $d/2H = 0.2$ to Fig. 12(b), $d/2H = 0.1$, one can see that at the same bulk Reynolds number $Re_B = 2600$, for $d/2H = 0.1$ the temperature spikes in the wake region are almost not observed. This confirmation is also supported by comparison of DNS (Fig. 14(a)) to experimental results, shown in Fig. 14(b). The experiments were performed at $d/2H = 0.07$, and in Fig. 14(b) one cannot observe the appearance of spikes behind the sphere.

While in the experiment at $Re_B = 8650$, only one spike was observed, the DNS at $Re_B = 2600$ showed three spikes. We believed that the low Reynolds number in the simulations compared to the experiments is the cause of such inconsistency. To examine this question we discuss the ex-

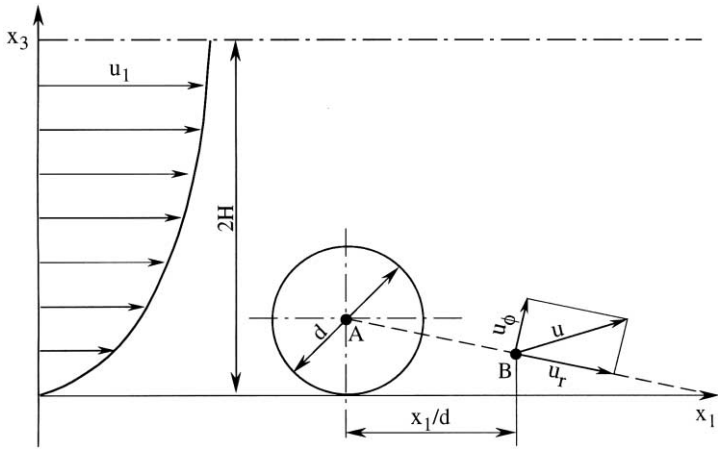

Fig. 15. Schematic description of the flow behind the sphere.

perimental results available in the literature for flow past an obstacle at a low Reynolds number. The temperature field on the bottom of a channel, in the wake of a rib placed in the spanwise direction was studied at $Re_B = 3100$ by Hetsroni et al. (1997a). The distribution of the heat transfer coefficient was non-monotonically and showed several spikes. The latter was probably due to the interaction of macro-scale vortices downstream of the rib and the bottom of the flume. The experimental results of the distributions of the local convective heat transfer in a flow at $1000 < Re_B < 5500$ over cubes mounted at one of the walls of a plane channel was presented by Meinders et al. (1998). The variations in the local convective heat transfer were attributed to quasi-periodic motions which were caused by vortex shedding. The strong velocity fluctuations normal to the wall cause the convective heat transfer intensification. The flow reattachment should be accompanied by a low value of the heat transfer coefficient.

4.3. Physical model

To estimate the effect of the change of the velocity vector on the heat transfer coefficient, consider the DNS results shown in Figs. 7–13. In domain 1 (Fig. 16), the average velocity decreases. This is clearly observed in the vector plot of the velocity field in the $x_1^+ - x_3^+$ and $x_1^+ - x_2^+$ planes the velocity decreases, beginning from x_1^+ about 450 (Fig. 7) and x_1^+ about 480 (Fig. 8) for the sphere $d^+ = 34$ and $d^+ = 17$, respectively. Under these conditions the rate of heat transfer coefficient decreases. It can be observed in Figs. 10 and 11 at x_{1C}/d from -10 to -2. Obviously this effect is more pronounced when the ratio $d/2H$ increases (Fig. 11).

Although the absolute value of velocity vector decreases also in the domain 2, the DNS shows that the variation of the heat transfer coefficient is qualitatively different from the above explanation. The dominant factor in the heat transfer enhancement is the effect of centrifugal forces on the structure of turbulent flow. Consider the near-wall flow in front of the sphere. From Figs. 7(a) and 8(a) one can see that the streamlines are inclined to the bottom of the flume. In this case motion of a fluid element from its position to the wall is accompanied by fluctuation growth, due to the excess centrifugal force. It is well known that in a stationary curved flow, the centrifugal forces acting on a fluid element affect heat transfer. These effects manifest themselves clearly in flows in curved channels, where the heat transfer coefficient near the concave wall is large than

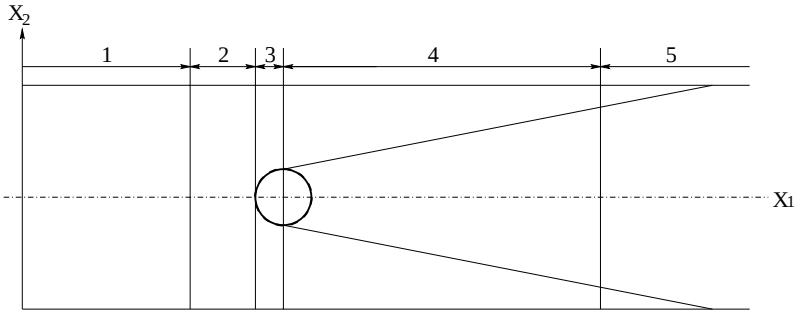

Fig. 16. Sketch of the flow pattern analyzed for heat transfer: Zone 1 – decreased flow, a long way from the sphere; Zone 2 – strong flow toward the bottom in the vicinity of the front of the sphere; Zone 3 – weak flow toward the bottom; Zone 4 – unstable flow; Zone 5 – downstream wake.

that near the convex wall. For the sphere (in the region located near the front) the rate of heat transfer is determined by strong enough flow toward the bottom, which causes sharp growth of the heat transfer coefficient. Zone 3 corresponds to the domain where the flow toward the bottom is week, and the heat transfer coefficient decreases up to the first minimum at $x_{1C}/d \sim 0$. In the region 4 ($0 < x_{1C}/d < 6$, zone of the unstable flow behind the sphere) the interaction of the wake behind the sphere with turbulent boundary layer is accompanied by an intermitted momentum and heat transfer. It was shown by Hetsroni et al. (1997a) that in this region the unperturbed (without the sphere) regular flow structure (periodic in the spanwise direction) may be represented as a combination of an irregular flow and a flow in which restoration of the regular flow structure takes place. In Zone 5 the disturbances are damped, and with increase of x_{1C}/d the heat transfer coefficient approached its value in unperturbed flow.

5. Conclusions

The DNS study of the flow characteristics around a single sphere submerged in turbulent flow in a water flume ($Pr = 5.4$) was performed. Two-way coupling was used to account for the effect of the sphere on the structure of the near-wall turbulence and main stream. The heat transfer calculations were carried out at a constant heat flux wall boundary condition. For the particle attached to the bottom of the flume the calculation shows a cooler area in the front of the particle and a cooler tail in its wake. Variation of heat transfer coefficient for water flow agrees well with experimental results presented in the literature. The DNS results indicate the essential enhancement of heat transfer coefficient due to the presence of the sphere. This effect is more pronounced in the region within about two sphere diameters from the center of the sphere. The influence of a sphere $d^+ = 34$ is much greater than that of a sphere $d^+ = 17$, and the heat transfer is much more turbulent and fluctuated behind the larger sphere $d^+ = 34$. It was shown that a decrease of bottom temperature is associated with a flow motion toward the wall, whereas an increase of it is associated with a motion away from the wall.

Acknowledgements

This research was supported by the Basic Research Foundation administered by the Israel Academy of Sciences and Humanities and by the Ministry of Science, State of Israel. The Research was also supported by the Fund for the Promotion of Research at the Technion. A. Mosyak is partially supported by the Ministry of Absorption, State of Israel. C.-F. Li is supported by the Council for Higher Education in Israel, and I. Tiselj was supported by a grant from the Lady Davis Foundation.

References

Chyu, M.K., Natarajan, V., 1991. Local heat/mass transfer distributions on the surface of a wall-mounted cube. Trans. ASME, J. Heat Transfer 113, 851–857.

Dasgupta, A., Guenard, P., Ultman, J.S., Kimbell, J.S., Morgan, K.T., 1993. A photographic method for visualization of mass uptake patterns in aqueous systems. Int. J. Heat Mass Transfer 36, 453–462.

Davalath, J., Bayazitoglu, Y., 1987. Forced convection cooling across rectangular blocks. Trans. ASME, J. Heat Transfer 109, 321–328.

Faghri, M., Asako, Y., 1994. Prediction of turbulent three-dimensional heat transfer of a heated blocks using low-Reynolds number two-equation model. Number Heat Transfer 26, 87–101.

Fisher, E.M., Eibeck, P.A., 1990. The influence of a horseshoe vortex on local convective heat transfer. Trans. ASME, J. Heat Transfer 112, 329–335.

Goldstein, D., Handler, R., Sirovich, L., 1993. Modeling a no-slip flow boundary with an external force field. J. Comput. Phys 105, 354–366.

Goldstein, R.J., Karni, J., 1984. The effect of a wall boundary layer on local mass from a cylinder in cross-flow. Trans. ASME, J. Heat Transfer 106, 260–267.

Goldstein, R.J., Chyu, M.K., Hain, R.C., 1985. Measurement of local mass transfer on a surface in the region of the base of a protruding cylinder with computer controlled data acquisition system. Int. J. Heat Mass Transfer 28, 977–985.

Hetsroni, G., Gurevich, M., Rozenblit, R., Yarin, L.P, Ziskind, G., 2001. The effect of particle motion on the thermal structure and on the heat transfer. Int. J. Multiphase Flow 27, 393–413.

Hetsroni, G., Mosyak, A., Yarin, L.P., 1997a. Thermal streaks regeneration in the wake of a disturbance in a turbulent boundary layer. Int. J. Heat Mass Transfer 40, 4161–4168.

Hetsroni, G., Rozenblit, R., Yarin, L.P., 1997b. The effect of coarse particles on the heat transfer in a turbulent boundary layer. Int. J. Heat Mass Transfer 40, 2201–2217.

Hetsroni, G., Rozenblit, R., 1994. Heat transfer to a liquid–solid mixture in a flume. Int. J. Multiphase Flow 20, 671–689.

Hetsroni, G., Rozenblit, R., Lu, D.M., 1995. Heat transfer enhancement by a particle on the bottom of a flume. Int. J. Multiphase Flow 21, 963–984.

Hussaini, M.Y., Zhang, T.A., 1987. Spectral methods in fluid dynamics. Annu. Rev. Fluid Mech. 19, 339–367.

Ichimiya, K., Akino, N., Kunugi, T., Mitsushiro, K., 1988. Fundamental study of heat transfer and flow situation around a spacer (in the case of a cylindrical rod as spacer). Int. J. Heat Mass Transfer 31, 2215–2225.

Igarashi, T., Yamasaki, H., 1989. Fluid flow and heat transfer of a rectangular cylinder in the turbulent boundary layer on a plate. Trans. JSME 55B, 3157–3165.

Iritani, Y., Kasagi, N., Hirata, M., 1984. Heat transfer mechanism and associated turbulence structure in the near-wall region of a turbulence boundary layer. In: Bradbury, L.J.S., et al. (Ed.), Turbulent Shear Flow. Springer, Berlin, pp. 223–234.

Kasagi, N., Kuroda, A., Hirata, M., 1989. Numerical investigation of near-wall turbulent heat transfer taking into account the unsteady heat conduction in the solid wall. Trans. ASME, J. Heat Transfer 111, 385–392.

Kasagi, N., Tomita, Y., Kuroda, A., 1992. Direct numerical simulation of the passive scalar field in a turbulent channel flow. Trans. ASME, J. Heat Transfer 114, 598–606.

Kawamura, H., Ohsaka, K., Abe, H., Yamamoto, K., 1998. DNS of turbulent heat transfer in channel flow with low to medium-high Prandtl number fluid. Int. J. Heat Fluid Flow 19, 482–491.

Kim, J., Moin P, , Moser R, 1987. Turbulence statistics in fully developed turbulent channel flow at low Reynolds number. J. Fluid Mech. 177, 133–166.

Kong, H., Choi, H., Lee, J.S., 2000. Direct numerical simulation of turbulent thermal boundary layers. Phys. Fluids 12, 2555–2568.

Kurose, R., Komori, S., 1999. Drag and lift forces on a rotating sphere in a linear shear flow. J. Fluid Mech. 384, 183–206.

Lam, K.L., Banerjee, S., 1988. Investigation of turbulent flow bounded by a wall and a free surface. In: Michandelides, E.E., Sharma, M.P. (Eds.), Fundamentals of Gas–Liquid Flows, vol. 72. ASME, Washington, DC, pp. 29–38.

LeVeque, R.J., 1992. Numerical Methods for Conservation Laws. Birkhäuser, Basel, Lectures in Mathematics, ETH, Zurich.

Li, C., Mosyak, A., Hetsroni, G., 1999. Direct numerical simulation of particle turbulence interaction. Int. J. Multiphase Flow 25, 187–200.

Li, C.F., Hetsroni, G., Mosyak, A., 2000. The influence of Prandtl number on heat transfer around a sphere placed in a turbulence boundary layer. In: Cheng, P. (Ed.), Proceedings of Symposium on Energy Engineering in the 21st Century. Hong Kong, pp. 255–261.

Lu, D.M., Hetsroni, G., 1995. Direct numerical simulation of a turbulent channel flow with heat transfer. Int. J. Heat Mass Transfer 38, 3241–3251.

McLaughlin, J.B., 1991. Inertial migration of a small sphere in linear shear flows. J. Fluid Mech. 224, 261–274.

Meinders, E.R, Hanjalic, K, Van der Meer, T.H., 1998. Similarity and dissimilarity between the surface heat transfer and the flow structure in turbulent flows over surface-mounted cubes. In: Proceedings of 11th International Heat Transfer Conference, vol. 3. Kyongju, Korea, pp. 51–56.

Morris, G.K., Garimella, S.V., 1996. Thermal wake downstream of a three-dimensional obstacle. Exp. Therm. Fluid Sci. 12, 65–74.

Na, Y., Hanratty, T.J., 2000. Limiting behavior of turbulent scalar transport close to a wall. Int. J. Heat Mass Transfer 43, 1749–1758.

Nakajima, M., Ota, T., 1998. Numerical simulation of three-dimensional unsteady flow and heat transfer around a surface-mounted hexahedron in a channel in heat transfer. In: Proceedings of 11th International Heat Transfer Conference, vol. 3. Kyongju, Korea, pp. 133–138.

Pan, Y., Banerjee, S., 1996. Numerical simulation of particle interactions with turbulence. Phys. Fluids 8, 2733–2755.

Saffman, P.G., 1965. The lift on a small sphere in a slow shear flows. J. Fluid Mech. 22, 385–400.

Schlosser, P.M., Godo, M.N., Fornes, T.D., Hubal, E.C., 1998. Application of a photographic method for determining mass transfer to flow around a submerged parallelepiped. Int. J. Heat Mass Transfer 41, 2991–3004.

Sparrow, E.M., Yanezmoreno, A.A, Otis Jr., D.R, 1984. Convective heat transfer response to height differences in an array of block-like electronic components. Int. J. Heat Mass Transfer 27, 469–473.

Tiselj, I., Pogrebnyak, E., Mosyak, A., Hetsroni, G., 2000. Numerical study of thermal streak spacing in turbulent boundary with constant heat-flux boundary condition. In: Proceedings of the ASME-ZSITS International Thermal Science Seminar. Bled, Slovenia, pp. 177–183.

Zhang, X., Stasiek, J., Collins, M.W., 1995. Experimental and numerical analysis of convective heat transfer in turbulent channel flow with square and circular columns. Exp. Therm. Fluid Sci. 10, 229–237.

Zukauskas, A., Slanciauskas, A., 1987. In: Karni, J. (Ed.), Heat Transfer in Turbulent Fluid Flows. Springer, Berlin, New York, Paris.